Increasing the metal loading in passion fruit-like nano-architectures

Rosa D'Apice, Valerio Voliani*

Center for Nanotechnology Innovation @NEST, Istituto Italiano di Tecnologia, P.zza San Silvestro, 12 – 56126 - Pisa (PI), Italy

*Corresponding author: E-mail: valerio.voliani@iit.it

Received: 07 February 2017, Revised: 20 March 2017 and Accepted: 09 April 2017

DOI: 10.5185/amlett.2017.1668
www.vbripress.com/aml

Abstract

Noble metal nanostructures have demonstrated many intriguing features for both therapy and diagnosis in a number of diseases. However, their clinical translation is prevented by their accumulation in organisms that can result in toxicity and interference with common medical diagnoses. In order to combine the most interesting behaviour of metal nanoparticles with the possibility of their body clearance, we have recently introduced and tested the passion fruit-like nano-architectures. They are versatile 100 nm biodegradable nanostructures composed by a silica shell embedding functional polymeric arrays of ultra-small noble metal nanoparticles. Here, we report a novel simple and robust protocol to increase the loading of ultra small gold nanoparticles in the nano-architectures, promoting their possible application in clinical diagnosis.

Keywords: Metal nanoparticles, biodegradable, nanomedicine, drug delivery, diagnosis, silica.

Introduction

The ability to engineer the geometry and surface coating of metal nanoparticles has resulted in a number of promising nanostructures with diagnostic and therapeutic functionality thanks to their peculiar chemical, physical and physiological features [**1–5**]. On the other hand, their average diameter is usually over 20 nm, resulting in a common fate of accumulation in liver and spleen [**6, 7**]. Indeed, the threshold for renal excretion, the most efficient clearance pathway, is 6 nm [**8**]. Larger objects can be excreted by liver and spleen into the biliary pathway, but the process for intact metal nanoparticles is slow and inefficient, resulting in metal accumulation [**9**, **10**].

This is one of the main concerns for the clinical translation of metal nanoparticles, indeed the US Food and Drug Administration requires that agents injected into the human body should be cleared completely in a reasonable amount of time, avoiding persistence in the organism [**10**]. This requisite is currently not fulfilled by any metal based nanoparticle [**6**].

One approach to overcome the issue of metal persistence is by decreasing the diameter of inorganic nanoparticles to few nanometers, in order to meet the ideal fast clearance through kidneys [**10, 11**]. However, ultrasmall metal nanoparticles usually lose the unique features and functionalities of bigger nanostructures, and an excessively fast clearance hampers their therapeutic and diagnostic applications [**8**].

Thus, the optimal equilibrium on the particle size for clinical applications is still an unresolved issue [**6**, **7**, **12**]. An elegant approach to fill the gap between promising metal nanomaterials and oncology is the composition of hybrid disassembling nanomaterials [**13**]. Upon their controlled in vivo disassembly into smaller non-toxic fragments, they are rapidly cleared via kidney, bladder and urine [**7**].

In this direction, we have introduced a modular system that combines the optical behavior of metal nanoparticles with a potentially complete body clearance [**13, 14**]. The 100 nm nano-architectures are composed by a silica nanocapsule comprising in the cavity functional polymeric arrays of ultrasmall metal nanoparticles showing an average diameter of 3 nm. The silica shell protects the material in the inner cavity from the environment and provide a simple functionalizable surface, the polymer is modifiable by standard protocols with dyes, drugs and chelating agents, while metal nanoparticles confer the optical and physical behavior needed for imaging applications [**14, 15**]. It is noticeable that the nano-architectures biodegrade in physiological media and cells in few days to silicic acid, GSH-coated ultrasmall metal nanoparticles and non-toxic polymers [**14, 16, 17**]. Thus, the degradation products of these nano-architectures are compatible with the possibility to overcome metal accumulation thank to the renal clearance of the building blocks.

The content of metal in passion fruit-like nano-architectures obtained by using the standard protocol is

usually the 5.9±1.3% w/w on the weight of freeze-dried samples [**13, 14, 18**]. This quantity can be not enough for some kind of imaging techniques, such as X-rays imaging [**19**]. Here, in order to overcome this issue, we report an updated protocol to produce passion fruit-like nano-architectures with a tripled content of ultrasmall metal nanoparticles.

Experimental

Materials

Hydrogen tetrachloroaurate (III) trihydrate was purchased by Alfa Aesar and used without further purification. All the other chemicals were obtained by Sigma-Aldrich.

Material synthesis

Synthesis of AuNPs

AuNPs with a diameter of approximately 3 nm were prepared according to the following procedure. To 20 mL of milliQ water were added 10 μL of poly(sodium 4-styrene sulfonate) 70kDa (30% aqueous solution) and 200 μL of $HAuCl_4$ aqueous solution 25mM. During vigorously stirring, 200 μL of $NaBH_4$ (4 mg/mL in milliQ water) were added quickly, and the mixture was stirred vigorously for other 2 minutes. After the addition of $NaBH_4$, the solution underwent some color changes until becoming brilliant orange. Before its use the solution was generally aged for at least 30 minutes and employed without further purification.

Synthesis of AuNPs arrays

To 20 mL of AuNPs solution were added 200 μL of poly(L-lysine) hydrobromide 15-30 kDa milliQ solution (20 mg/ml) and the mixture was allowed to stir for 30 minutes at room temperature. The as synthesized AuNPs aggregates were collected by centrifugation (13400 rpm for 3 minutes), suspended in 2 mL of milliQ water and sonicated for maximum 4 minutes.

Synthesis of AuSi

In a 100 mL round bottomed flask was added 70 mL of absolute ethanol followed by 2.4 mL of ammonium hydroxide solution (30% in water), and 40 μL of tetraethyl orthosilicate (TEOS, 98%). The solution was allowed to stir for 20 minutes at RT. 2 mL of the AuNPs arrays previously prepared were added to the reaction flask and the solution was allowed to stir for further 3h at RT. The as-synthesized AuSi were collected by 30-minute centrifugation at 4000 rpm, washed twice with ethanol to remove unreacted precursors and suspended in 1 mL of ethanol. A short spin centrifugation was employed in order to separate the structures over 150 nm from the supernatant, which was recovered as a pink- iridescent solution. The solution was centrifuged at 13400 rpm for 5 minutes, suspended in 500 μL milliQ water, sonicated for 5 minutes and freeze-dried overnight. Usually, about 1.5 mg of a brilliant pink powder is obtained, which remains stable for at least 1 year if stored sealed in the dark at 10 ˚C.

Synthesis of AuSiT and AuSiC

The synthesis of passion fruit-like nano-architectures showing a thinner silica shell respect to standard AuSi (AuSiT) and cookies-like nanoparticles (AuSiC) were performed by reducing the quantity of TEOS and modifying the time-addition of the polymeric arrays of AuNPs as in the following. In a 100 mL round bottomed flask were added 70 mL of absolute ethanol followed by 2.4 mL of ammonium hydroxide solution (30% in water), and 10 μL of tetraethyl orthosilicate (TEOS, 98%). In order to obtain AuSiT or AuSiC, 2 mL of AuNPs arrays were added to the reaction flask after, respectively, 30 or 5 minute. The solution was then allowed to stir for further 3h at RT. The as-synthesized nano-architectures were collected by 25 minute centrifugation at 4000 rpm, washed twice with ethanol to remove unreacted precursors and suspended in 1 mL of ethanol. A short spin centrifugation was employed in order to separate the structure over 150 nm from the supernatant, which was recovered as a pink-iridescent solution. The solution was centrifuged at 13400 rpm for 5 minutes, suspended in 500 μL milliQ water, sonicated for 5 minutes and freeze-dried overnight. Usually, about 0.5 mg of a brilliant pink powder is obtained, which remains stable for at least 1 year if stored sealed in the dark at 10 ˚C.

Characterizations

UV/Vis spectrophotometry

Extinction spectra were collected by means of a double beam spectrophotometer Jasco V-550 UV/VIS equipped with quartz cuvettes of 1 cm path length and normalized to the maximum absorbance. MilliQ water was employed as solvent.

Electron microscopy

TEM observations of nanoparticles: measurements were carried out on a ZEISS Libra 120 TEM operating at an accelerating voltage of 120 kV, equipped with an in-column omega filter. The colloidal solutions were deposited on 300-mesh carbon-coated copper grids and air dried overnight before being imaged.

ICP-MS Analysis

Nanoparticles were dissolved in 1 mL aqua regia (prepared with ICP-MS grade HCl and HNO3) and digested under microwave irradiation (200 °C/15 minutes) in Teflon-lined vessels. The resulting solution was diluted to 10 mL with ICP-MS grade water, and content of Au was determined by ICP-MS analysis against a standard calibration curve.

Results and discussion

The general synthetic strategy employed for the preparation of passion fruit-like nano-architectures (AuSi) is reported in **Fig. 1a**. Gold nanoparticles (AuNPs) of 2.8±0.4 nm coated by negative poly(sodium 4-styrene sulfonate) (PSS) were aggregated in spherical arrays by positive 15-30 kDa poly(L-lysine) (PL) by means of ionic interactions.

Then, the silica shell was grown on this template by a modified Stöber method, resulting in 100 nm nano-architectures **(Fig. 1b)** [**13**]. The composition of the silica shell around gold arrays is related to the simultaneous presence of both amines from PL and aromatic moieties from PSS [**14**]. Indeed, aromatic additives have been demonstrated to be required also for the formation of a silica shell around PL templates in the synthesis of hollow silica microspheres [**20**]. The investigation on the silica shell formation mechanism was reported elsewhere [**14**].

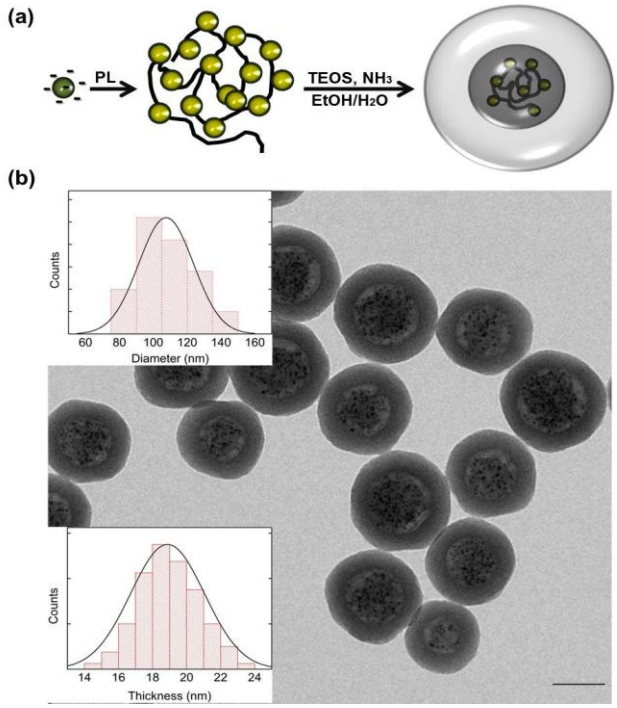

Fig. 1. a) scheme for the general synthesis of AuSi AuSiT, and AuSiC. Negative ultrasmall gold nanoparticles are assembled in spherical array employing poly(L-lysine), and these polymeric arrays are then embedded in hollow silica shells. b) Typical TEM image of AuSi, scalebar: 50 nm. Size distribution histograms of AuSi diameter (upper inset), and of their wall thickness (bottom inset). All the histograms were made on measurements of at least 100 nanoparticles observed by TEM.

Briefly, tetraethoxysilane (TEOS) is hydrolyzed to orthosilicic acid and partially adsorbed into AuNPs polymeric arrays before/during its polymerization. Then, silica nuclei of 1–2 nm readily formed in solution, aggregate on the external surface of the arrays and the remaining orthosilicic acid continues to form a complete shell until its saturation limit is reached or the reaction interrupted (usually 3h). Interestingly, the concentration of gold nanoparticles in AuSi appears to decrease during the capsules formation, and the silica shell of the final capsules does not show gold nanoparticles inclusion. We suggest that a fraction of AuNPs are expelled during the consolidation of the shell.

By this standard synthetic approach are usually obtained passion fruit-like nano-architectures showing 107.6±16.1 nm in diameter, 18.9±2.2 nm of wall thickness, and containing 5.9±1.3% w/w of metal on the total weight of freeze-dried samples. AuSi are shown in **Fig. 1b**, and the insets report the diameter dispersion and wall thickness of at least 100 AuSi collected by TEM.

AuSi have demonstrated their biodegradation in physiological fluids and in cellular environment to potentially kidney-clearable building blocks, together with their application as endogenous-triggered drug carriers of cisplatin prodrug [**14**]. On the other hand, the metal loading of AuSi could be not enough for *in vivo* applications as biodegradable contrast agents or radio-sensitizers [**11, 21**].

The approaches to increase their metal loading can be essentially two: i) increase the concentration of AuNPs in AuSi, or ii) produce AuSi with a thinner silica shell. The first approach was not employable in our type of protocol. Moreover, we envisaged the second approach more suitable for the designed final applications.

It is useful to report here the mechanism of the standard Stöber synthesis [**22**]. The introduction of TEOS into the reaction medium is followed by its hydrolysis reactions, resulting in orthosilicic acid. The polymerization of orthosilicic acid occurs when the concentration exceeds the saturation limit in ethanol (about 0.02–0.03%) [**23**]. The process yields, in sequence, low- to high-molecular polymers and, thanks to their condensation, particles of 1–2 nm in diameter. Then nuclei increase in size following a LaMer growth pattern until their diameter reaches a critical value of 5–7 nm, after which they start to aggregate to form silica nanoparticles [**23**]. This process continues until the concentration of orthosilicic acid in the reaction medium exceeds the saturation limit.

In order to produce nano-architectures with a thinner silica shell and by keeping in mind the mechanisms of the standard and modified Stöber reactions, the quantity of TEOS in our standard protocol was reduced from 40 µL to 10 µL. Surprisingly, the nanoparticles produced by this approach were no more hollow, but cookies-like nanoparticles (AuSiC, data not shown). This can be probably ascribed to the fact that small silica nuclei request more time to be produced in presence of a reduced concentration of TEOS. Thus, the orthosilicic acid is fully adsorbed and polymerized directly inside the polymeric-gold arrays.

Thus, we employed another variation of the standard protocol together with the reduced TEOS: the addition of the AuNPs polymeric arrays to the reaction medium after 30 minutes. During this time, the silica nuclei and 5-7 nm silica nanoparticles are formed in the reaction medium. Thus, the delayed addition results in the aggregation of these silica nanomaterials on the outer surface of the polymeric-gold arrays for ionic interaction, and not in the

absorption of TEOS (or its hydrolyzed form) inside the arrays before its hydrolysis-condensation [**13**].

Then, the remaining orthosilicic acid continues to form a complete shell until its saturation limit is reached or the reaction interrupted. By this novel protocol, passion fruit-like nano-architectures with a thinner silica shell (AuSiT) were obtained, showing a diameter of 79.7±5.2 nm and a shell thickness of 11.1±1.1 nm **(Fig. 2a)**. It is worth to notice that the metal loading of AuSiT resulted to be 18±3% w/w on the total weight of freeze-dried samples.

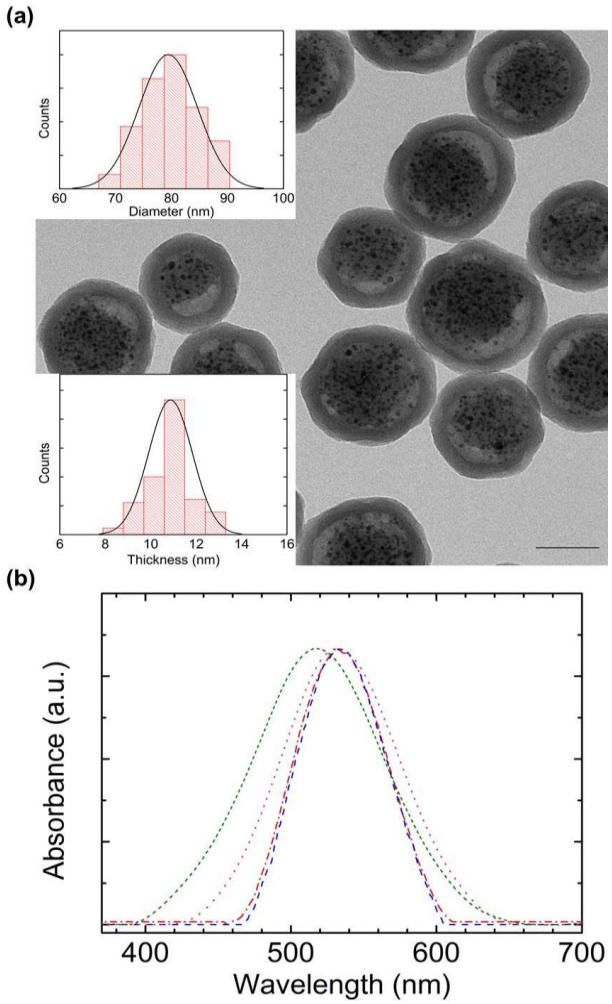

Fig. 2. a) Typical TEM image of AuSiT, scalebar: 50 nm. Size distribution histograms of AuSiT diameter (upper inset), and of their wall thickness (bottom inset). All the histograms were made on measurements of at least 100 nanoparticles observed by TEM. b) Spectral behavior of ultrasmall gold nanoparticles (green small dash), AuNPs polymeric arrays (pink dot), AuSi (red dash-dot), and AuSiT (blue dash). Spectra were collected in MilliQ water, normalized and the background subtracted.

The optical behavior of AuSi, AuSiT and their components are reported in **Fig. 2b**. The extinction band of AuNPs is around 514 nm. As expected, after the aggregation with PL, the band shifts to 539 nm due to the close proximity of AuNPs in the polymeric arrays [**13**]. After the formation of AuSi, the extinction band shifts to 532 nm, likely to an increased size-homogeneity of the processed nanostructures. Interestingly, AuSiT demonstrate an overlapping spectrum to AuSi, supporting the retention of the intriguing optical features of passion fruit-like nano-architectures.

Conclusion

In summary, we have presented a highly reproducible novel protocol for the production of passion fruit-like nano-architectures showing a thinner silica shell and an increased metal loading. Thanks to their peculiar physical and physiological behavior, these nanosystems are promising tools to overcome the issue of accumulation of inorganic nanoparticles in organisms and to fill the gap between metal nanoparticles and oncology. The development of this novel protocol paves the way for the application of passion fruit-like nano-architectures in imaging application requiring a high concentration of noble metals.

Acknowledgements

We thank Mr. Domenico Cassano for his support in the synthesis and helpful discussions, Dr. Giovanni Signore for his support in ICP-MS measurments and Dr. Mauro Gemmi for his support of the project.

Author's contributions

Conceived the plan: VV; Performed the expeirments: RD; Data analysis: RD and VV; Wrote the paper: VV. Authors have no competing financial interests.

References

1. Yang, X.; Yang, M.; Pang, B.; Vara, M.; Xia,Y.; Gold Nanomaterials at Work in Biomedicine, *Chem. Rev.*, **2015**, *115*, 10410. **DOI:**10.1021/acs.chemrev.5b00193
2. Dreaden, E. C.; Alkilany, A.M.; Huang, X.; Murphy, C. J.; El-Sayed, M. A., The golden age: gold nanoparticles for biomedicine, *Chem. Soc. Rev.*, **2012**, *41*, 2740. **DOI**:10.1039/C1CS15237H
3. Voliani,V.; Signore, G.; Vittorio, O.; Faraci, P.; Luin,S.; Peréz-,J.; Peréz-Prieto,J.; Beltram, F., Cancer phototherapy in living cells by multiphoton release of doxorubicin from gold nanospheres, *J. Mater. Chem. B.*, **2013**, *1*, 4225. **DOI:**10.1039/c3tb20798f
4. Vittorio, O.; Voliani, V.; Faraci, P.; Karmakar, B.; Iemma, F.; Hampel, S.; Kavallaris,M.; Cirillo, G., Magnetic Catechin-Dextran conjugate as targeted therapeutic for pancreatic tumour cells., *J. Drug Target.*, **2014**, *2330*, 1. **DOI:**10.3109/1061186X.2013.878941
5. Voliani, V.; Gemmi, M.; Francés-Soriano, L.; González-Béjar,M.; Pérez-Prieto, J., Texture and Phase Recognition Analysis of β-NaYF Nanocrystals, *J. Phys. Chem. C.*, **2014**, *118*, 11404. **DOI:**10.1021/jp5025872
6. Etheridge, M. L.; Campbell, S. A.; Erdman, A. G.; Haynes, C.L.; Wolf, S. M.; McCullough, J., The big picture on nanomedicine: the state of investigational and approved nanomedicine products., *Nanomedicine*, **2013**, *9*, 1. **DOI:**10.1016/j.nano.2012.05.013
7. K. Zarschler, L. Rocks, N. Licciardello, L. Boselli, E. Polo, K.P. Garcia, L. De Cola, H. Stephan, K. A. Dawson, Ultrasmall inorganic nanoparticles: state-of-the-art and perspectives for biomedical applications, Nanomedicine Nanotechnology, *Biol. Med.* **2016**, *12*, 1663. **DOI:**10.1016/j.nano.2016.02.019
8. T. Sun, Y.S. Zhang, B. Pang, D.C. Hyun, M. Yang, Y. Xia, Engineered Nanoparticles for Drug Delivery in Cancer Therapy, *Angew. Chemie Int. Ed.* **2014**, *53*, 12320. **DOI:**10.1002/anie.201403036

9. M. Yu, J. Zheng, Clearance Pathways and Tumor Targeting of Imaging Nanoparticles, *ACS Nano.*, **2015**, *9*, 6655. **DOI:**10.1021/acsnano.5b01320
10. H. Soo Choi, W. Liu, P. Misra, E. Tanaka, J.P. Zimmer, B. Itty Ipe, M.G. Bawendi, J. V Frangioni, Renal clearance of quantum dots, *Nat. Biotechnol.* **2007**, *25*, 1165. **DOI:**10.1038/nbt1340
11. C. Zhou, M. Long, Y. Qin, X. Sun, J. Zheng, Luminescent gold nanoparticles with efficient renal clearance., *Angew. Chem. Int. Ed. Engl.* **2011**, *50*, 3168. **DOI:**10.1002/anie.201007321
12. X.D. Zhang, J. Yang, S.S. Song, W. Long, J. Chen, X. Shen, H. Wang, Y.M. Sun, P.X. Liu, S. Fan, Passing through the renal clearance barrier: Toward ultrasmall sizes with stable ligands for potential clinical applications, *Int. J. Nanomedicine.*, **2014**, *9*, 2069. **DOI:**10.2147/IJN.S64301
13. D. Cassano, D. Rota Martir, G. Signore, V. Piazza, V. Voliani, Biodegradable hollow silica nanospheres containing gold nanoparticle arrays, *Chem. Commun.*, **2015**, *51*, 9939. **DOI:**10.1039/C5CC02771C
14. D. Cassano, M. Santi, V. Cappello, S. Luin, G. Signore, V. Voliani, Biodegradable Passion Fruit-Like Nano-Architectures as Carriers for Cisplatin Prodrug, *Part. Part. Syst. Charact.* **2016**, *33*, 818. **DOI:**10.1002/ppsc.201600175
15. C. Avigo, D. Cassano, C. Kusmic, V. Voliani, L. Menichetti, Enhanced Photoacoustic Signal of Passion Fruit-Like Nanoarchitectures in a Biological Environment, *J. Phys. Chem. C.* **2017**, *121*, 6955. **DOI:**10.1021/acs.jpcc.6b11799
16. E. Mahon, D.R. Hristov, K. a. Dawson, Stabilising fluorescent silica nanoparticles against dissolution effects for biological studies., *Chem. Commun. (Camb).* **2012**, *48*, 7970. **DOI:**10.1039/c2cc34023b
17. R. Kumar, I. Roy, T. Ohulchanskky, L. Vathy, In vivo biodistribution and clearance studies using multimodal organically modified silica nanoparticles, *ACS Nano.* **2010**, *4*, 699. **DOI:**10.1021/nn901146y
18. D. Cassano, J. David, S. Luin, V. Voliani, Passion fruit-like nano-architectures: a general synthesis route., *Sci. Rep.* **2017**, *7*, 43795. **DOI:**10.1038/srep43795
19. H. Lusic, M.W. Grinstaff, X-ray-Computed Tomography Contrast Agents, *Chem. Rev.* **2013**, *113*, 1641. **DOI:**10.1021/cr200358s
20. K. Van Bommel, J. Jung, S. Shinkai, Poly (L-lysine) Aggregates as Templates for the Formation of Hollow Silica Spheres, *Adv. Mater.* **2001**, *13*, 1472. **DOI:**10.1002/1521-4095(200110)13:19%3C1472::AID-ADMA1472%3E3.0.CO;2-L/abstract (accessed September 2, 2014)
21. Y.-S. Yang, R.P. Carney, F. Stellacci, D.J. Irvine, Enhancing Radiotherapy by Lipid Nanocapsule-Mediated Delivery of Amphiphilic Gold Nanoparticles to Intracellular Membranes, *ACS Nano.*, **2014**, *8*, 8992. **DOI:**10.1021/nn502146r
22. W. Stöber, A. Fink, E. Bohn, Controlled growth of monodisperse silica spheres in the micron size range, *J. Colloid Interface Sci.* **1968**, *26*, 62. **DOI:**10.1016/0021-9797(68)90272-5
23. V. M. Masalov, N.S. Sukhinina, E. a Kudrenko, G. a Emelchenko, Mechanism of formation and nanostructure of Stöber silica particles, *Nanotechnology*, **2011**, *22*, 275718. **DOI:**10.1088/0957-4484/22/27/275718

